DNS OF THE EVAPORATION OF ACETONE DROPLETS IN A SATURATED TURBULENT JET SPRAY

Federico Dalla Barba

Department of Industrial Engineering
University of Padova
Via Venezia 1, 35131, Padova, Italy
federico.dallabarba@unipd.it

Francesco Picano

Department of Industrial Engineering
University of Padova
Via Venezia 1, 35131, Padova, Italy
francesco.picano@unipd.it

ABSTRACT

The evaporation dynamics of liquid droplets dispersed within turbulent jets is crucial in a variety of industrial applications as well as from an environmental point of view. A typical examples consists in the improvement of engine combustion chambers. In this context, in order to improve the combustion efficiency and reduce pollutant emissions it is mandatory to better understand and control the spray evaporation dynamics. Indeed, this phenomenon has not been fully understood in the turbulent regime and existing models capabilities for applications are still limited. The present work aims to understand the physics of evaporating droplets within turbulent jets restricting to the non-reactive, dilute conditions. The crucial aspect of the present configuration is presence of dry air entrainment which affect the overall vaporization. The problem is addressed in a Direct Numerical Simulation framework adopting an hybrid Eulerian Lagrangian approach. A full coupling between the two phases is considered accounting for mass, momentum and energy exchanges. The distribution of droplets is found to be strongly non-homogeneous and preferential segregation is observed. This phenomenology affects the overall vaporization process and is responsible for a rapid increasing of droplets polidispersity.

INTRODUCTION

The evaporation of a turbulent spray of droplets involves several interplaying processes. As a liquid jet exits from a duct at high velocity, instabilities such as the Kelvin-Helmholtz and Rayleigh-Taylor develop and consequently fragmentize the jet into large drops or ligaments Jenny *et al.* (2012). Then aerodynamics forces acting on the liquid phase induce a further fragmentation until a dilute phase of small droplets takes place. In these conditions, droplets are so diluted in terms of volume fraction that their direct mutual interaction is negligible. In addition, the strong surface tension acting on small droplets make possible to model them as evaporating rigid spheres. However, their mass fraction can be significant such that their effect on the flow needs to be considered (two-way coupling conditions, Ferrante & Elghobashi (2003)). In this work we focus on these dilute conditions where a strong coupling among turbulence, inertial droplet dynamics and vapor concentration field is present. The finite inertia of the droplets may induce the formation of clusters where the local droplet concentration can be even hundreds time the bulk concentration. The high vapor concentration around a cluster may approach the saturation levels blocking the local evaporation Reveillon & Demoulin (2007). Conversely, the local forcing of the inertial droplets on the gas stirs the local gas velocity fluctuations. This micro-mixing may enhance the turbulent mixing around a cluster promoting the evaporation. The jet spray dynamics adds peculiar features on the evaporation process. A turbulent jet is characterized by a spreading and slowly decaying turbulent core surrounded by irrotational ambient gas. This (unsaturated) ambient gas is entrained in the core region and eventually dilutes it. This entrainment is crucial for droplet evaporation that is promoted by the incoming unsaturated gas. These aspects were never discussed in an evaporating spray jet at least with the richness of details given by a DNS and constitutes the main focus of the present work.

METHODOLOGY

The direct numerical simulation of the turbulent spray is addressed by an hybrid Eulerian/Lagrangian approach. The dynamics of the gaseous phase is described by a low Mach number formulation of the Navier-Stokes equations that accounts for density variations in the gaseous phase neglecting acoustics. Under the prescribed dilute conditions, droplets are treated as rigid evaporating spheres and the point-droplet approximation is adopted. Hence, three Lagrangian equations are considered in order to evolve droplets position, radius and temperature. In addition, a full coupling between the Lagrangian dispersed phase and the Eulerian gaseous phase is granted by three sink/source coupling terms in the right hand side of Navier-Stokes equations accounting for mass, momentum and energy exchange. Both the Lagrangian and Eulerian governing equations are consistent with those of previous studies in the field, (e.g. Miller & Bellan (1999); Bukhvostova *et al.* (2014)),

$$\frac{\partial \rho}{\partial t} + \nabla \cdot (\rho \mathbf{u}) = S_\rho \tag{1}$$

$$\frac{\partial}{\partial t}(\rho Y_V) + \nabla \cdot (\rho Y_V \mathbf{u}) = \nabla \cdot (\rho \mathscr{D} \nabla Y_V) + S_\rho \tag{2}$$

$$\frac{\partial}{\partial t}(\rho \mathbf{u}) + \nabla \cdot (\rho \mathbf{u} \otimes \mathbf{u}) = \nabla \cdot \boldsymbol{\tau} - \nabla P + \mathbf{S_m} \tag{3}$$

$$\nabla \cdot \mathbf{u} = \frac{1}{p_0}\left[\frac{\gamma - 1}{\gamma} \nabla \cdot (k \nabla T) + S_e\right] \tag{4}$$

$$p_0 = \rho \, R_G \left[1 + \left(\frac{W_G}{W_L} - 1\right) Y_V\right] T \tag{5}$$

$$\frac{d\mathbf{u_d}}{dt} = \frac{\mathbf{u} - \mathbf{u_d}}{\tau_d} \tag{6}$$

$$\frac{dm_d}{dt} = -\frac{1}{3}\frac{m_d}{\tau_d}\frac{Sh}{Sc} \, ln(1 + B_m) \tag{7}$$

$$\frac{dT_d}{dt} = \frac{1}{3\,\tau_d}\left(\frac{Nu}{Pr}\frac{C_{P,G}}{C_L}(T - T_d) - \frac{Sh}{Sc}\frac{L_V}{C_L} \, ln(1 + B_m)\right) \tag{8}$$

where ρ, $\mathbf{u}$, T, P and p_0 are respectively the gaseous phase density, velocity, temperature, hydrodynamic pressure and thermodynamic pressure. $Y_V = \rho_V / \rho$ is the vapor mass fraction field, defined as the ratio of the vapor partial density, ρ_V, and the gas phase global density.The thermodynamic pressure p_0 is constant in space, due to the low-Mach number asymptotic expansion (MAJDA &

Sethian (1985)) and in time, due to the open space conditions. The viscous stress tensor is $\tau = 2\mu(\nabla\mathbf{u} + \nabla\mathbf{u}^T) - 2\mu_b/3\ \nabla\cdot\mathbf{u}\ \mathbf{I}$, with μ and μ_b the dynamic and bulk viscosities. The parameter $\mathscr{D}$, k, γ, W_G, W_L and $R_G = \bar{R}/W_G$ are respectively the vapor/gas binary diffusion coefficient, the thermal conductivity and the specific heat ratio of the vapor/gas mixture, the molar mass of gas and liquid and the gas specific constant. The mass, momentum and energy coupling terms are S_ρ, S_m and S_e (see e.g. Mashayek (1998)). In the Lagrangian equations 6 - 8, $\mathbf{u}_d$, m_d and T_d are the droplet velocity, mass and temperature while $C_{P,G}$, C_L and L_V are the specific heat at constant pressure of the gas, the specific heat of the liquid and the latent heat of vaporization. The time-dimension parameter $\tau_d = 2\rho_L r_d^2/(9\mu)$ is the droplet relaxation time, with ρ_L the liquid density and r_d the droplet radius. The mass diffusivity and thermal conductivity are expressed in terms of the Schmidt and Prandtl numbers, $Sc = \mu/(\rho\mathscr{D})$, $Pr = \mu/(C_P k)$. The mass and heat transfer ratio due to convection are accounted through the Sherwood and Nusselt numbers estimated according to the Frössling correlation:

$$Nu_0 = 2 + 0.552\ Re_d^{\frac{1}{2}}\ Pr^{\frac{1}{3}} \tag{9}$$

$$Sh_0 = 2 + 0.552\ Re_d^{\frac{1}{2}}\ Pr^{\frac{1}{3}} \tag{10}$$

where $Re_d = \rho||\mathbf{u}_d - \mathbf{u}||2\ r_d/\mu$ is the droplet Reynolds number. These latter are corrected according to Abramzon & Sirignano (1989) in order to account for the Stefan flow effect:

$$Nu = 2 + \frac{(Nu_0 - 2)}{F_T}, \qquad F_T = \frac{(1+B_t)^{0.7}}{B_t}\ ln(1+B_t) \tag{11}$$

$$Sh = 2 + \frac{(Sh_0 - 2)}{F_M}, \qquad F_M = \frac{(1+B_m)^{0.7}}{B_m}\ ln(1+B_m) \tag{12}$$

where B_m and B_t are the Spalding mass and heat transfer numbers:

$$B_m = \frac{(Y_{V,s} - Y_V)}{(1 - Y_{V,s})} \tag{13}$$

$$B_t = \frac{C_{P,V}}{L_V}(T - T_d) \tag{14}$$

with $C_{P,V}$ the vapor specific heat at constant pressure. In correspondence of the droplet surface a saturation condition establishes so that the vapor mass fraction is $Y_{V,s} = \rho_{V,s}/\rho$ with $\rho_{V,s}$ the vapor partial density at saturation (evaluated at droplet temperature). If the equilibrium hypothesis is assumed, the vapor molar fraction in the vapor/gas saturated mixture at droplet surface, $\chi_{V,s}$, can be estimated by the Clausius-Clapeyron relation and $Y_{V,s}$ follows immediately:

$$\chi_{V,s} = \frac{p_{ref}}{p_0} exp\left[\frac{L_V}{R_V}\left(\frac{1}{T_{ref}} - \frac{1}{T_d}\right)\right] \tag{15}$$

$$Y_{V,s} = \frac{\chi_{V,s}}{\chi_{V,s} + (1 - \chi_{V,s})\frac{W_g}{W_L}} \tag{16}$$

with p_{ref} and T_{ref} arbitrary reference pressure and temperature and $R_V = \bar{R}/W_L$ the vapor specific constant.

T	273.15 K	ψ_l	0.05
p_0	101300 Pa	ψ_t	0.23
ρ	1.3 kg/m^3	U	9 m/s
ν	1.5 $10^{-5} m^2/s$	R	5 10^{-3} m

Table 1. Main environmental and physical parameters of the DNS. T, ρ and ν are respectively the temperature, density and kinematic viscosity of the gaseous phase at the inlet section. p_0 is the environmental thermodynamic pressure. R and U are the inlet radius and bulk velocity. $\psi_l = \dot{m}_l/\dot{m}_g$ is the injected liquid acetone mass fraction defined as the ratio between the liquid acetone and air mass flow rates. $\psi_t = (\dot{m}_l + \dot{m}_v)/\dot{m}_g$ is the total injected acetone mass fraction, with $\dot{m}_v$ the mass flow rate of acetone vapor.

In this paper we report the Direct Numerical Simulation of an evaporating air/acetone turbulent spray. The gaseous carrier phase is composed by a mixture of dry air and acetone vapor while droplets are entirely composed by liquid acetone. The computational domain consists of a cylinder coaxial to the spray axis, extending for $2\pi \times 22R \times 70R$ in the azimuthal, θ, radial, r and axial, z, directions. The domain discretization is based on a non-equispaced, staggered mesh in the radial and axial direction composed by $N_\theta \times N_r \times N_z = 128 \times 255 \times 640$ nodes. An Eulerian algorithm directly solves equations 1 - 5 on the cylindrical domain (see e.g. Picano *et al.* (2011); Rocco *et al.* (2015) and references therein for validation and testing). A second order central finite differences scheme is adopted on the staggered grid for space discretization, while temporal evolution is performed by a low-storage third order Runge- Kutta scheme. A Lagrangian solver evolves droplets mass, momentum and temperature laws 6 - 8 using the same time-integration algorithm. The gaseous turbulent flow is injected throughout a center orifice at one base of the domain. A time-dependent inlet condition (Dirichlet) is prescribed by using a cross-sectional plane of a periodic turbulent pipe flow, provided by a companion time-evolving DNS. This grants a fully turbulent inflow velocity. The remaining part of the domain base is impermeable and adiabatic. A convective condition is adopted at the outlet and an adiabatic traction-free condition is prescribed at the side boundary in order to make the entrainment of external dry air possible. The injection flow rate of the gas is kept constant fixing a bulk Reynolds number $Re = 2UR/\nu = 6000$, with U the bulk velocity, R the inlet radius and ν the kinematic viscosity. A nearly-saturated condition is prescribed for the air/acetone vapor mixture at the inflow section, $S = Y_V/Y_{V,s} = 0.99$, with S the saturation field defined as the ratio of actual vapor mass fraction and the saturated vapor mass fraction at actual temperature $Y_{V,s} = Y_{V,s}(T)$. Liquid monodisperse acetone droplets with radius $r_{d,0} = 6\mu m$ are injected within the saturated vapor carrier phase. The injected droplets are distributed randomly over the inflow section with initial velocity equals to the local turbulent gas phase velocity. Other simulation parameters are reported in table 1.

The code capabilities in reproducing droplets vaporization dynamics have been tested in two different cases. The former considers a water droplet evaporating within a laminar dry air jet. In these extremely dilute conditions the droplet is subjected to constant surrounding vapor concentration and equation 7 can be analytically integrated. The solution is the so called d^2 law:

$$r_d = \sqrt{r_{d,0}^2 - kt} \qquad k = \frac{2\rho\mathscr{D}\ ln(1+B_m)}{\rho_L} \tag{17}$$

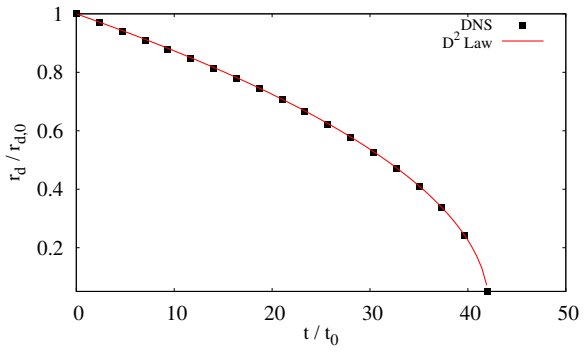

(a)

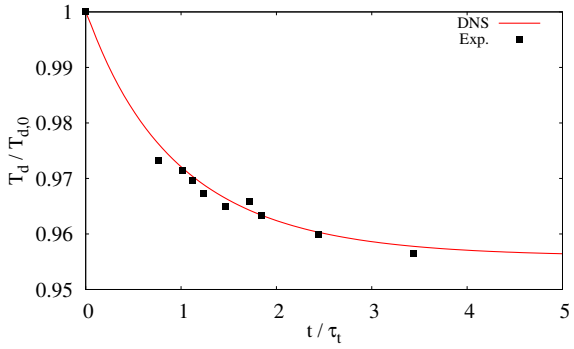

(b)

Figure 1. (a) Time evolution of the radius of a single water droplet in a dry air laminar jet. The environmental pressure and temperature are $p = 101300Pa$ and $T = 273.15K$. The inlet radius and the bulk velocity of the jet are $R = 5\ 10^{-3}\ m$ and $U = 1.7m/s$. The initial droplet radius is set to $r_{d,0} = 5\mu m$ while temperature and velocity are the same of the gaseous carrier phase. The radius and the time are scaled by the droplet initial radius, $r_{d,0}$, and the reference time scale $t_0 = R/U$ respectively. The numerical solution (dots) is compared to the d^2 law 17 (continuous line). (b) Time evolution of the temperature of a water droplet freely falling in air. Pressure, temperature and relative humidity are $p = 101300Pa$, $T = 301.45K$ and $\chi = 0.22$. Droplet is initially at rest at the ambient temperature. The temperature and time are scaled by the initial droplet temperature, $T_{d,0}$, and by the droplet thermal relaxation time, τ_t, defined as the time required by droplet temperature to change by the 63 % of its total change. The numerical solution (continuous line) is compared to the experimental dataset (dots).

The comparison between the numerical and the analytical solution are provided in Figure 1(a). In the second validation test, a water droplet freely falling in wet air has been considered. The temperature of droplet is initially set to the environmental air one and changes during the fall until settling on the ventilated wet bulb temperature. The evolution of droplet temperature has been compared to experimental measurements (Kinzer & Gunn (1951)) in Figure 1(b).

The Eulerian solver has been validated performing a DNS of droplet-free air/acetone vapor jet in the same conditions prescribed for the droplet-laden simulation. In the far-field of a turbulent jet the average centerline axial velocity is known to evolve proportionally to the inverse of the axial distance from the inlet:

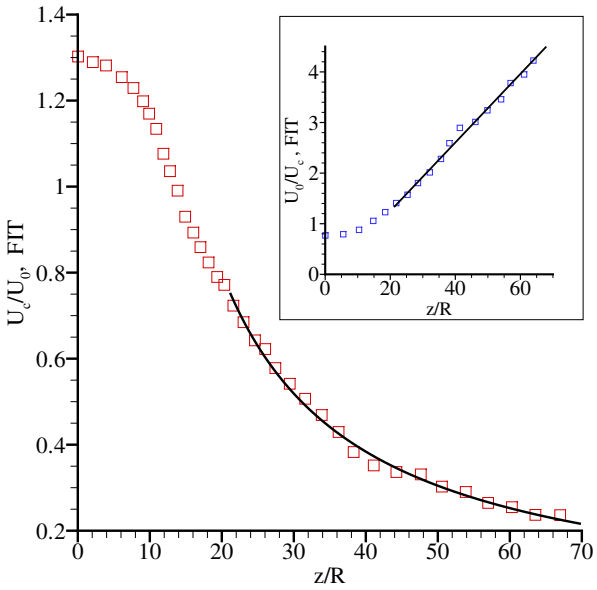

Figure 2. Average of the non-dimensional centerline axial velocity of the jet, U_c/U_0 (main frame) and its inverse (inset). The reference velocity scale is the inlet bulk velocity, $U_0 = 9\ m/s$. The square represents the numerical data while the continuous line corresponds to the linear fitting of U_0/U_c. The virtual origin and the velocity decaying factor estimated through the linear interpolation are respectively $B \simeq 7$ and $z_0 \simeq 0$.

$$\frac{U_c}{U} = \frac{B}{z/D - z_0/D} \tag{18}$$

where B is an empirical constant and z_0 is the so-called virtual origin representing the location of an equivalent point source of momentum originating the jet in far field. Figure 2 report the numerically computed evolution of the centerline velocity compared to that resulting from relation 18. The decaying factor and the virtual origin has been found to be $B \sim 7$ and $z_0 \sim 0$ respectively, that are consistent with the values reported in literature for fully turbulent inlet conditions (see e.g. Hussein *et al.* (1994); Webster *et al.* (2001)).

RESULTS AND DISCUSSION

Figure 3(a) shows the overall behavior of the turbulent jet spray providing a snapshots of the vapor mass fraction field and of droplets position through an axial cut of the cylindrical domain. Droplets are non-homogeneously distributed over the spray and clustering is also apparent. More specifically, in the jet core droplets tend to preferentially segregate within zones with higher vapor phase concentration (see Figure 3(b)), while the outer part of the jet is depleted of droplets. This organization of the liquid phase strongly affects the overall evaporation dynamics, leading to the average liquid mass fraction distribution reported in Figure 4(a). The 50 % of liquid mass transits to vapor phase between the inflow section and $z/R \simeq 20$. In order to estimate the vaporization length an arbitrary threshold of 0.1% is fixed on the ratio between the residual liquid and the injected liquid mass fraction. According to this criterion, the vaporization process is completely terminated at $z/R \simeq 43$. It should be noted that in correspondence of each axial distance from inlet the mass fraction is higher in the spray core and lower in

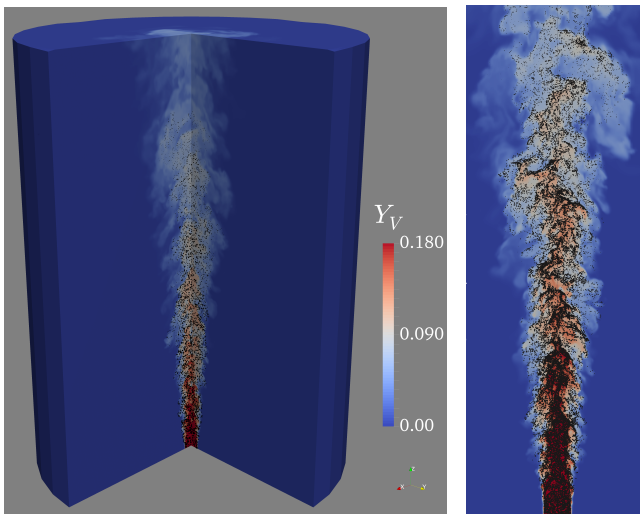

(a) (b)

Figure 3. (a) An instantaneous snapshot of the 3D computational domain. The overall spray behavior is visible through the axial cut. The contour plot shows the vapor mass fraction field, Y_V, that ranges between the saturation value prescribed at inlet, $Y_V = 0.18$, and the dry air value, $Y_V = 0$. A random sample of 250000 droplets within the whole 5 10^6 droplets population is represented by black points. Each point size is proportional to the corresponding droplet radius with a scale factor 200. (b) A radial-axial slice of the spray. The contour plot shows the vapor mass fraction field (same range of box (a)) while black points represent droplets (same sample of box (a)).

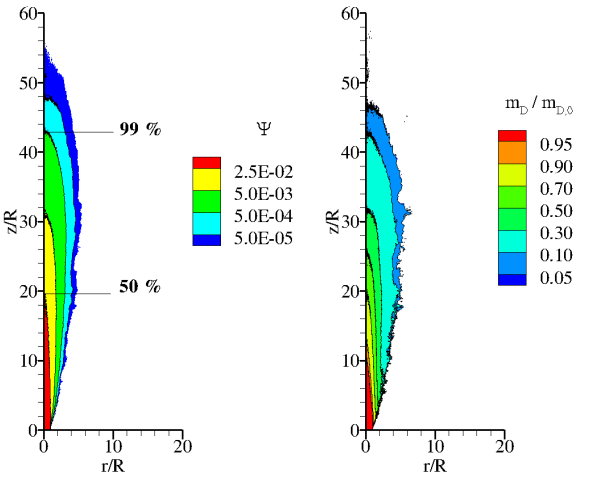

(a) (b)

Figure 4. (a) Average liquid mass fraction field, $\psi_l = m_l/m_g$ with m_l and m_g the liquid and gas mass inside a small control volume ΔV. The labels show the axial distances from inlet where the 50% and 99% of the injected liquid mass has evaporated. (b) Average non-dimensional droplets mass, $m_d/m_{d,0}$. The reference mass scale is the droplets initial mass $m_{d,0}$.

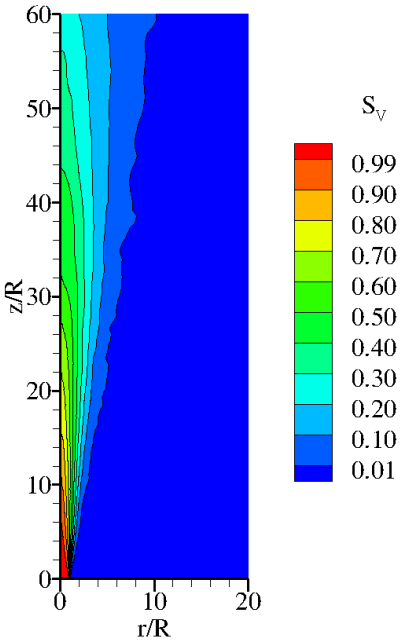

Figure 5. Average acetone vapor saturation field, $S = Y_V/Y_{V,s}$, where Y_V is the actual vapor mass fraction and $Y_{V,s}(T)$ is the value of the vapor mass fraction at saturation estimated through relation 16 at the local actual temperature.

the external mixing layer. The same trend is followed by the average droplets mass distribution reported in Figure 4(b), where a progressive decreasing of average droplets sizes can be observed moving away from the jet axis.

In the overall spray evolution, this behavior can be explained since the turbulent jet is vapor-saturated and large part of droplets evaporation occurs in the shear layer of the outer region where dry air entrainment occurs. In a turbulent spray indeed, the turbulent core is continuously entrained by the dry environmental gas (da Silva *et al.* (2014)) which dilutes the vapor concentration in the mixing layer playing a fundamental role in sustaining the vaporization process. Hence droplets that reach this region can fully evaporate disappearing from the field. In the inner jet core, instead, droplets may survive for long time when surrounded by a cloud of highly concentrated vapor. The effect of dry air entrainment can be observed in Figure 5 showing the average saturation field. At the inflow section the saturation field assumes the prescribed near-unit value, decreasing slowly in the downstream evolution of the spray. Since the inner fluid can not reach the outer spray layer, the dilution effect is more intense in this latter region. As a consequence, the vaporization process advance at a higher rate in the mixing layer then in the spray core. This is consistent with the previously described mass distribution.

The decreasing vapor concentration that droplets *feel* in their downstream evolution is mainly responsible for the deviation of the time-evolution of average droplets square diameter from the d^2 law. Figure 6 shows the average square diameter of droplets injected simultaneously as a function of time. Between the inflow section and $z/R \simeq 30$, the actual trend of d_d^2 follows approximatively the trend of the d^2 law. Further downstream the vaporization process accelerates and the d^2 law overestimates the actual value of d_d^2. We explain this behavior considering the high vapor concentration downstream the inflow section. In this region, the most part of droplets are located in the spray core and flow away surrounded by approximatively constant average vapor concentration. Moving downstream the dilution effect caused by the dry environmental air entrainment becomes more significant causing the acceleration of the overall vaporization process.

In contrast with boost exerted by entrainment on the vaporization of the liquid phase, the preferential segregation of droplets

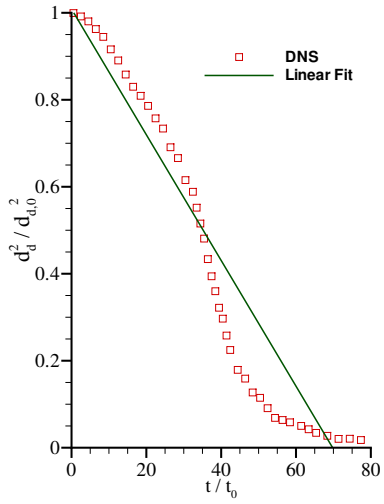

Figure 6. The plot provides the average square diameters of droplets injected simultaneously as a function of time (squares). Each variable is non-dimensional. The reference length and time scales are the initial droplets diameter, $d_{d,0}$, and the reference time, $t_0 = R/U$, with R the inlet radius and U the bulk velocity. The continuous line represent a linear fit of the actual $d_d^2/d_{d,0}^2$ trend corresponding to the d^2 law trend described by relation 17.

within highly saturated regions tends to decrease the vaporization rate especially in the spray core. In order to quantify this effect, we have compared two different statistics for the vapor mass fraction field: the Eulerian mean, Y_V, and the mean of the vapor mass fraction sampled by droplets, $Y_{V,ds}$, defined as the average of the vapor mass fraction conditioned by the presence of a droplet at a fixed location. Thus, wherever droplets preferentially accumulate inside high vapor concentration regions, it results $Y_{V,ds} > Y_V$. Figure 7(a) and 7(b) provide the trend of these statistics as a function of the radial distance from the jet axis at respectively $z/R = 15$ and $z/R = 30$. Around $z/R = 15$ the vapor mass fraction sampled by droplets and the correspondent unconditional value are similar with the exception of the outer spray layer. Further downstream the preferential sampling of the vapor phase concentration operated by droplet becomes significant even in the inner jet core. This is indicative of how the most part of droplets evaporate inside clusters where the average local vapor concentration is sensibly higher then its bulk value. Moreover, droplets moving towards the outer, droplets-free, environment are entrapped into turbulent structures with high vapor concentration, this giving the main contribution to the oversampling of the vapor concentration field in the outer mixing layer. Since the vaporization rate of droplets is driven by the vapor concentration sampled by droplets themselves, this oversampling phenomenology results in a slowdown of the vaporization process, thus increasing the overall vaporization length and time with respect to the estimate given by the unconditional vapor phase mean concentration.

The previously described dynamics result in an intense spreading of the droplet radius spectrum in the downstream evolution of the spray. The probability density function (PDF) of the droplets radius at different distances from the origin is provided in figure 8(a). Even starting from a monodisperse distribution, we observe that the PDF of droplets radius spans over around one decade after 10 jet radii from the inlet. It should be remarked that this quantity amounts in differences of droplet volumes of about 10^3. The evolution of droplets dynamics is indeed strongly affected by the time-history of the vapor concentration *felt* by each droplets. This is in turns ex-

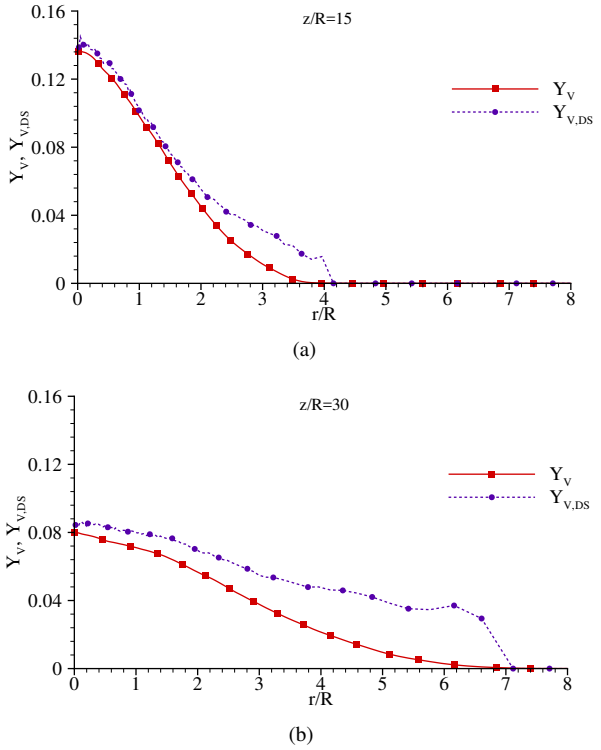

Figure 7. The figures provide the radial distribution of the Eulerian mean of the vapor mass fraction field, Y_V, and the mean of the vapor mass fraction sampled by droplets, $Y_{V,ds}$. Figure (a) corresponds to an axial distance from the jet inlet of $z/R = 15$ while figure (b) of $z/R = 30$.

tremely different over droplets population due to the complex preferential segregation dynamics. Figure 8(b) provides the probability density function of the vapor saturation field sampled by droplets at different axial distances from inlet. This correspond to the driving parameter of the vaporization rate. Immediately downstream the inflow section, the saturation field ranges from $S \simeq 0.3$ to $S \simeq 1$ due to the simultaneous presence of droplets populating the saturated spray core and the nearly dry mixing layer. In the downstream evolution. the saturation fields distribution spread increases exceeding 1, this corresponding to the presence of condensation events. Moving further downstream, ($z/R \simeq 20$) the spreading trend inverts and droplets are subjected to progressively more uniform saturation levels.

FINAL REMARKS

In this paper, we address the Direct Numerical Simulation of a turbulent evaporating spray in dilute, non-reacting conditions. An hybrid Eulerian-Lagrangian approach is adopted and a full coupling between the two phases is considered accounting for mass, momentum and energy exchange. The simulation reproduces a saturated air/acetone vapor jet laden with liquid monodisperse acetone droplets at a bulk Reynolds number of $Re = UR/\nu = 6000$. The effect of dry environmental air entrainment is also accounted. We found that the distribution of droplets population over the spray is strongly non-homogeneous and clustering is apparent. Droplets preferential segregation strongly affect the overall vaporization process, reducing the overall vaporization rate and thus increasing the overall vaporization length and time. In order to quantify the effect of droplets preferential segregation on the vaporization process we have considered the mean of the vapor mass fraction field sampled by droplets. The preferential segregation dynamics, indeed,

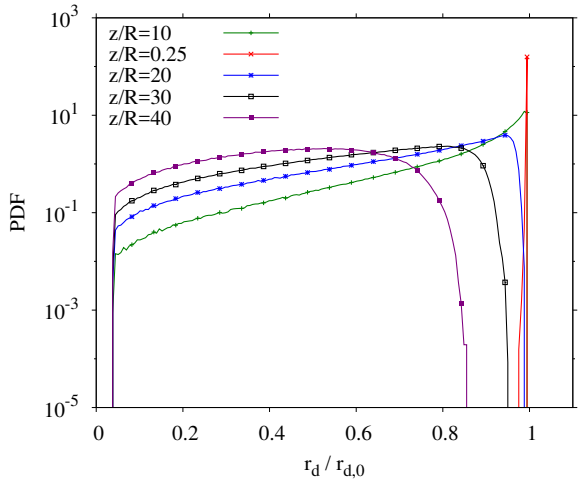

(a)

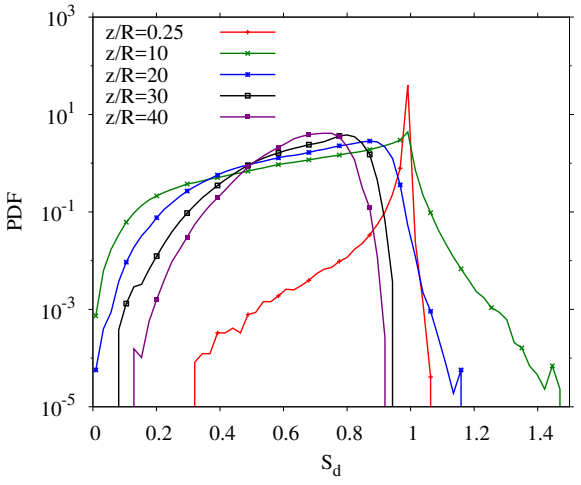

(b)

Figure 8. (a) Probability density function of droplet radius computed over 5 different samples of the entire droplets population. Each sample is constitute by droplets located within a cylindrical cut of the domain of width $s/R = 0.1$ centered at different axial distances from inlet, z/R. (b) Probability density function of the saturation field sampled by droplets computed over the same samples of figure (a).

is responsible for a significant increasing of this statistics with respect to its unconditional mean value. In addition, we observed an extremely rapid increasing of droplets polidispersity in the downstream evolution of the spray. Even starting from a monodisperse distribution, the probability density function of droplets radius is found to span over around one decade even at only 10 jet radii downstream the inlet section. This mechanisms, related to droplets extremely non-homogeneous dynamics, is expected to be crucial in affecting the dynamics of all droplet-laden turbulent flows characterized by a mixing layer with entrainment of dry air such as for turbulent warm clouds.

Acknowledgement

The authors would like to acknowledge the financial support through the University of Padova Grant PRAT2015 (CPDA154914) as well as the computer resources provided by CINECA ISCRA C project TaStE (HP10CCB69W) and the contribution of the COST Action Flowing Matter (MP1305).

REFERENCES

Abramzon, B & Sirignano, WA 1989 Droplet vaporization model for spray combustion calculations. *International journal of heat and mass transfer* **32** (9), 1605–1618.

Battista, F, Picano, F, Troiani, G & Casciola, Carlo Massimo 2011 Intermittent features of inertial particle distributions in turbulent premixed flames. *Physics of Fluids* **23** (12), 123304.

Bec, Jeremie, Biferale, Luca, Cencini, Massimo, Lanotte, Alessandra, Musacchio, Stefano & Toschi, Federico 2007 Heavy particle concentration in turbulence at dissipative and inertial scales. *Physical review letters* **98** (8), 084502.

Bukhvostova, A, Russo, E, Kuerten, JGM & Geurts, BJ 2014 Comparison of dns of compressible and incompressible turbulent droplet-laden heated channel flow with phase transition. *International journal of multiphase flow* **63**, 68–81.

Ferrante, Antonino & Elghobashi, Said 2003 On the physical mechanisms of two-way coupling in particle-laden isotropic turbulence. *Physics of fluids* **15** (2), 315–329.

Hussein, Hussein J, Capp, Steven P & George, William K 1994 Velocity measurements in a high-reynolds-number, momentum-conserving, axisymmetric, turbulent jet. *Journal of Fluid Mechanics* **258**, 31–75.

Jenny, Patrick, Roekaerts, Dirk & Beishuizen, Nijso 2012 Modeling of turbulent dilute spray combustion. *Progress in Energy and Combustion Science* **38** (6), 846–887.

Kinzer, Gilbert D & Gunn, Ross 1951 The evaporation, temperature and thermal relaxation-time of freely falling waterdrops. *Journal of Meteorology* **8** (2), 71–83.

MAJDA, ANDFREW & Sethian, James 1985 The derivation and numerical solution of the equations for zero mach number combustion. *Combustion science and technology* **42** (3-4), 185–205.

Mashayek, F 1998 Direct numerical simulations of evaporating droplet dispersion in forced low mach number turbulence. *International journal of heat and mass transfer* **41** (17), 2601–2617.

Miller, Richard S & Bellan, J 1999 Direct numerical simulation of a confined three-dimensional gas mixing layer with one evaporating hydrocarbon-droplet-laden stream. *Journal of Fluid Mechanics* **384**, 293–338.

Picano, F, Battista, F, Troiani, G & Casciola, Carlo Massimo 2011 Dynamics of piv seeding particles in turbulent premixed flames. *Experiments in Fluids* **50** (1), 75–88.

Reveillon, Julien & Demoulin, François-Xavier 2007 Effects of the preferential segregation of droplets on evaporation and turbulent mixing. *Journal of Fluid Mechanics* **583**, 273–302.

Rocco, G, Battista, F, Picano, F, Troiani, G & Casciola, Carlo Massimo 2015 Curvature effects in turbulent premixed flames of h2/air: a dns study with reduced chemistry. *Flow, Turbulence and Combustion* **94** (2), 359–379.

da Silva, Carlos B, Hunt, Julian CR, Eames, Ian & Westerweel, Jerry 2014 Interfacial layers between regions of different turbulence intensity. *Annual review of fluid mechanics* **46**, 567–590.

Webster, DR, Roberts, PJW & Ra'ad, L 2001 Simultaneous dptv/plif measurements of a turbulent jet. *Experiments in Fluids* **30** (1), 65–72.